Atmos. Chem. Phys. Discuss., 15, 11889–11923, 2015
www.atmos-chem-phys-discuss.net/15/11889/2015/
doi:10.5194/acpd-15-11889-2015

Atmospheric Chemistry and Physics Discussions
Open Access

On the statistical optimality of CO_2 atmospheric inversions assimilating CO_2 column retrievals

F. Chevallier

Laboratoire des Sciences du Climat et de l'Environnement, CEA-CNRS-UVSQ, L'Orme des Merisiers, Bat 701, 91191 Gif-sur-Yvette, France

Received: 2 March 2015 – Accepted: 8 April 2015 – Published: 22 April 2015

Correspondence to: F. Chevallier (frederic.chevallier@lsce.ipsl.fr)

Published by Copernicus Publications on behalf of the European Geosciences Union.

Abstract

The extending archive of the Greenhouse Gases Observing SATellite (GOSAT) measurements (now covering about six years) allows increasingly robust statistics to be computed, that document the performance of the corresponding retrievals of the column-average dry air-mole fraction of CO_2 (XCO_2). Here, we compare a model simulation constrained by surface air-sample measurements with one of the GOSAT retrieval products (NASA's ACOS). The retrieval-minus-model differences result from various error sources, both in the retrievals and in the simulation: we discuss the plausibility of the origin of the major patterns. We find systematic retrieval errors over the dark surfaces of high-latitude lands and over African savannahs. More importantly, we also find a systematic over-fit of the GOSAT radiances by the retrievals over land for the high-gain detector mode, which is the usual observation mode. The over-fit is partially compensated by the retrieval bias-correction. These issues are likely common to other retrieval products and may explain some of the surprising and inconsistent CO_2 atmospheric inversion results obtained with the existing GOSAT retrieval products. We suggest that reducing the observation weight in the retrieval schemes (for instance so that retrieval increments to the retrieval prior values are halved for the studied retrieval product) would significantly improve the retrieval quality and reduce the need for (or at least reduce the complexity of) ad-hoc retrieval bias correction. More generally, we demonstrate that atmospheric inversions cannot be rigorously optimal when assimilating XCO_2 retrievals, even with averaging kernels.

1 Introduction

CO_2 surface fluxes at the Earth's surface can be inferred from accurate surface measurements of CO_2 concentrations, but the sparseness of the current global network still leaves the flux horizontal and temporal gradients, and even their latitudinal distribution, very uncertain (Peylin et al., 2013). This limitation has provided a major in-

ACPD
15, 11889–11923, 2015

centive to develop the monitoring of CO_2 concentrations from space. First retrievals were obtained from existing instruments measuring either the thermal infrared radiation emitted by the atmosphere (Chédin et al., 2003) or the reflected sunlight in the near-infrared (NIR)/shortwave infrared (SWIR) spectral regions (Buchwitz et al., 2005). The latter technique allows retrieving XCO_2 while the former is not sensitive to CO_2 in the lower atmosphere, near the CO_2 sources and sinks. Since active (lidar) measurement techniques for XCO_2 from space are still in development (e.g., Ingmann et al., 2009), NIR/SWIR measurements currently offer the best prospect to provide "retrievals of CO_2 of sufficient quality to estimate regional sources and sinks", as phrased by objective A.8.1 of the Global Climate Observing System programme (GCOS, 2010), in the short term. However, they are hampered by uncertain knowledge about scatterers in the atmosphere at the corresponding wavelengths (aerosols and cirrus clouds) with an effect that varies with surface albedo, which is itself uncertain (e.g., Aben et al., 2007). Such interference in the XCO_2 signal seen in the NIR/SWIR measurements is of concern because even sub-ppm systematic errors (corresponding to less than 0.25 % of the signal) can severely flaw the inversion of CO_2 surface fluxes (Chevallier et al., 2007; Miller et al., 2007). This risk motivated dedicated developments of the retrieval algorithms in order to de-convolve the spectral signatures of the involved compounds as much as possible (e.g., Reuter et al., 2010; Guerlet et al., 2013b).

The Japanese GOSAT, launched in January 2009, and the USA second Orbiting Carbon Observatory (OCO-2), launched in July 2014, observe the NIR/SWIR radiation with unprecedented spectral resolution in order to specifically address this remote sensing challenge. The GOSAT archive already covers nearly six years and can provide good insight into the adequacy of NIR/SWIR retrievals for CO_2 source-sink inversion. In terms of random errors, raw GOSAT retrievals now reach single shot precision better than 2 ppm (one sigma) in favourable measurement conditions (e.g., Nguyen et al., 2014). This performance is better than what pre-launch studies suggested: for instance Maksuytov et al. (2008) expected 2.5–10 ppm single shot precision only. Systematic errors are difficult to quantify or else they would be removed. They are likely

ACPD
15, 11889–11923, 2015

state-dependent with absolute values varying in time and space about the ppm before any bias correction (Nguyen et al., 2014). They also depend on the retrieval algorithm (e.g., Oshchepkov, 2013). As expected, the remaining uncertainty has profound impact on CO_2 source-sink inversions (Basu et al., 2013; Chevallier et al., 2014), but XCO_2 retrievals have already served as a basis to study the carbon budgets of some regions (Guerlet et al., 2013a; Basu et al., 2014; Reuter et al., 2014). For instance, 25 scientists analysed several XCO_2 retrievals over continental Europe and concluded that the current understanding of the European carbon sink brought by bottom-up inventories had to be revisited (Reuter et al., 2014).

This paper aims at contributing to the debate about the relevance of current GOSAT retrievals for atmospheric inversions. Our starting point is a critical review of the basic principles behind the current processing chains that go in successive steps from GOSAT measured radiance spectra to surface flux estimates (Sect. 3). We then focus on the GOSAT retrievals provided by NASA's Atmospheric CO_2 Observations from Space project (ACOS, build 3.4, described in Sect. 2) for the period between June 2009 and May 2013. They are of particular interest because they have been processed in a way that prefigures the official OCO-2 retrievals in terms of spectral bands and available simultaneous observations (O'Dell et al., 2012). In Sect. 4, we analyse the residuals between the ACOS-GOSAT retrievals and the simulated CO_2 concentration fields of the Monitoring Atmospheric Chemistry and Climate atmospheric inversion product (MACC, version 13r1, also described in Sect. 2) that assimilated surface air sample measurements from various networks. Concluding discussion follows in Sect. 5.

2 Retrievals and model simulation

2.1 ACOS-GOSAT retrievals

GOSAT is a joint venture by the Japan Aerospace Exploration Agency (JAXA), the National Institute for Environmental Studies (NIES) and the Ministry of the Environment

ACPD
15, 11889–11923, 2015

(MOE) in Japan. This spacecraft is operated in a sun-synchronous polar orbit that crosses the Equator at about 13:00 LT during daytime and that repeats every 3 days. As described by O'Dell et al. (2012) and Osterman et al. (2013), the ACOS algorithm retrieves XCO_2 from a selection of GOSAT measurements of reflected sunlight made in the same spectral bands than OCO-2. Over land, such measurements are made by pointing the instrument to the Earth on both sides of the satellite track. Given the low reflectivity of water surfaces, ocean measurements are only possible when the instrument is pointed to the sun-glint spot, which is only done within 40° from the Equator in the summer hemisphere. GOSAT also carries a cloud and aerosol imager that can help filtering difficult scenes out, but unlike other GOSAT retrieval algorithms, ACOS does not use it since OCO-2 does not contain a similar instrument.

Following Boesch et al. (2006) and Connor et al. (2008), the ACOS algorithm relies on optimal estimation (i.e. Bayesian methods) to retrieve the vertical profile of the CO_2 dry air mole fraction together with variables interfering in the measurements: the surface pressure and the surface albedo, some variables describing temperature, water vapour, clouds and aerosols in the atmosphere, and channel offsets for the instrument. The retrieved XCO_2 is simply obtained by integrating the retrieved CO_2 profile. In this Bayesian formulation of the retrieval, prior information about CO_2 is given an artificially small weight in order to maximize the observation contribution to the result: for instance, the standard deviation of the uncertainty assigned to the prior XCO_2 is larger than 10 ppm (O'Dell et al., 2012), i.e. larger than typical variations of XCO_2 at the continental scale (e.g., Keppel-Aleks et al., 2011). We will discuss the impact of this choice later and for simplicity, we will call XCO_2^b and XCO_2^a the prior (*background*) and the retrieved (*analysed*) XCO_2, respectively. XCO_2^a can be compared with model simulations, as will be done here, or with other measurements via the associated CO_2 averaging kernel profiles and prior profiles (e.g., Connor et al., 1994). For nadir viewing, XCO_2^a is representative of a volume that has a circular footprint at the Earth's surface of diameter about 10 km.

ACPD
15, 11889–11923, 2015

Previous comparisons between XCO_2^a and model simulations or reference ground-based XCO_2 measurements from Total Carbon Column Observing Network (TCCON) highlighted some systematic dependency of the error of XCO_2^a as a function of a series of internal variables of the algorithm (Wunch et al., 2011b). This feature reveals some limitations of the algorithm but also allows correcting them empirically, for instance before they are assimilated in atmospheric inversion systems (Crisp et al., 2012). We will call $XCO_2^{a,c}$ the bias-corrected retrievals.

2.2 MACC CO_2 inversion

Since year 2011, the MACC pre-operational service (www.copernicus-atmosphere.eu) has been delivering a CO_2 inversion product with biannual updates. Release 13r1 primarily describes the CO_2 surface fluxes over more than three decades, from 1979 to 2013, at resolution 3.75° × 1.9° (longitude–latitude) and 3 hourly, based on 131 CO_2 dry air mole fraction station records from three large databases:

- the NOAA Earth System Research Laboratory archive (NOAA CCGG, http://www.esrl.noaa.gov/gmd/ccgg/index.html),
- the World Data Centre for Greenhouse Gases archive (WDCGG, http://ds.data.jma.go.jp/gmd/wdcgg/),
- the Réseau Atmosphérique de Mesure des Composés à Effet de Serre database (RAMCES, http://www.lsce.ipsl.fr/).

The three databases include both in situ measurements made by automated quasi-continuous analysers and irregular air samples collected in flasks and later analyzed in central facilities. The detailed list of sites is provided in Tables 1 and 2.

The MACC Bayesian inversion method is formulated in a variational way in order to estimate the CO_2 surface fluxes at the above-described relatively high resolution over the globe (Chevallier et al., 2005, 2010). For v13r1, the system used a single 35 year inversion window, therefore enforcing physical and statistical consistency in the inverted fluxes. Fluxes and mole fractions are linked in the system by the global atmospheric transport model of the Laboratoire de Météorologie Dynamique (LMDZ, Hourdin et al., 2006) with 39 layers in the vertical and with the same horizontal resolution than the inverted fluxes. LMDZ is nudged to ECMWF-analysed winds for flux inversion.

The MACC inversion product also contains the 4-D CO_2 field that is associated to the inverted surface fluxes through the LMDZ transport model. Simulating the GOSAT retrievals from this field is nearly straight-forward. The only difficulty lies in the interpolation from the LMDZ 39-level vertical grid to the 20-level vertical grid of the retrievals, before the retrieval averaging kernels are applied. Indeed, the model orography at resolution $3.75^\circ \times 1.9^\circ$ significantly differs from the high-resolution orography seen by the retrievals. For the interpolation, we assume that CO_2 concentrations vary linearly with the pressure in the vertical. When the model surface pressure is smaller than the retrieved surface pressure, the profile is artificially extended at constant value below the model surface. In the opposite case, model levels below the sounding surface are ignored. We compensate this artificial change of mass in the profile by systematically adjusting the interpolated profile so that its pressure-weighted mean equals that of the profile before the interpolation.

3 Theoretical aspects

Like the other retrieval and inversion systems (see, e.g., Oshchepkov et al., 2013; Peylin et al., 2013), ACOS-GOSAT and MACC both follow the Bayesian paradigm in its Gaussian linear form (e.g., Rodgers, 2000) in order to estimate the most likely state, in a statistical sense, of the CO_2 profile and of the CO_2 surface fluxes, respectively. In mathematical terms, given $\boldsymbol{x}$ the vector that gathers the variables to be inferred (either a 1-D CO_2 profile or 2-D+1-D CO_2 surface fluxes), given $\boldsymbol{x}^b$ an a priori value of $\boldsymbol{x}$ (coming from a climatology or from a model), and given $\boldsymbol{y}$ the vector that gathers all relevant observations (either radiances or retrievals), the most likely state of $\boldsymbol{x}$ is

ACPD
15, 11889–11923, 2015

written:

$$\boldsymbol{x}^{a} = \boldsymbol{x}^{b} + \mathbf{K}(\boldsymbol{y} - \mathbf{H}\boldsymbol{x}^{b}) \tag{1}$$

$\mathbf{H}$ a linearized observation operator that links variables $\boldsymbol{x}$ and $\boldsymbol{y}$ (i.e. essentially a radiative transfer model or a transport model). $\mathbf{K}$ is the following "Kalman gain" matrix:

$$\mathbf{K} = \mathbf{B}\mathbf{H}^{T}(\mathbf{H}\mathbf{B}\mathbf{H}^{T} + \mathbf{R})^{-1} \tag{2}$$

$\mathbf{B}$ and $\mathbf{R}$ are the error covariance matrices of $\boldsymbol{x}^{b}$ and $\boldsymbol{y}$, respectively.

The error covariance matrix of $\boldsymbol{x}^{a}$ is obtained by:

$$\mathbf{A} = (\mathbf{I} - \mathbf{K}\mathbf{H})\mathbf{B} \tag{3}$$

with $\mathbf{I}$ the identity matrix with appropriate dimension.

For simplicity, Eq. (1) does not make other variables that are simultaneously inferred appear, like clouds, aerosols or surface variables for the retrievals, or the 3-D state of CO_2 at the start of the inversion window for the inversion.

The current processing chains that go from radiances to surface fluxes are two-step processes. We now distinguish the retrieval process and the inversion process by putting breves $\breve{}$ on all symbols related to the former and hats $\hat{}$ on all symbols related to the latter. In a first step, the CO_2 profiles and their uncertainty $\breve{\boldsymbol{x}}$, $\breve{\mathbf{A}}$ are retrieved for each sounding separately. The resulting ensemble forms the observations to be simultaneously assimilated $\widehat{\boldsymbol{y}}$, $\widehat{\mathbf{R}}$ for the second step. The presence of prior information $\boldsymbol{x}^{b}$ in both steps complicates the transition between the two. Following Connor et al. (1994), we can technically eliminate the influence of $\breve{\boldsymbol{x}}^{b}$ (but not of its uncertainty) by the following adaptation of Eq. (1) in the second step: we subtract the retrieval prior $\breve{\boldsymbol{x}}^{b}$ from each CO_2 profile simulated by the transport model at the sounding location $\widehat{\mathbf{H}}\widehat{\boldsymbol{x}}^{b}$, we multiply the result by the retrieval averaging kernel matrix $\breve{\mathbf{K}}\breve{\mathbf{H}}$ and finally add $\breve{\boldsymbol{x}}^{b}$. The retrieval error covariance matrix should consistently be diminished (e.g., Connor et al., 2008, paragraph 37). We call $\widehat{\mathbf{H}}'$ the convolution of the transport model operator with

Discussion Paper | Discussion Paper | Discussion Paper | Discussion Paper |
ACPD
15, 11889–11923, 2015
On the optimality of satellite-based CO_2 atmospheric inversions
F. Chevallier
Title Page
Abstract Introduction
Conclusions References
Tables Figures
◄ ►
Back Close
Full Screen / Esc
Printer-friendly Version
Interactive Discussion

the individual retrieval averaging kernels and $\widehat{\mathbf{R}}'$ the adjusted retrieval error covariance matrix. By applying Eq. (1) twice and after accounting for the above adaptation, the processing chain can be written in a concise form:

$$\widehat{\boldsymbol{x}}^{\mathrm{a}} = \widehat{\boldsymbol{x}}^{\mathrm{b}} + \widehat{\mathbf{K}}\breve{\mathbf{K}}\left(\breve{\boldsymbol{y}} - \breve{\mathbf{H}}\widehat{\mathbf{H}}'\widehat{\boldsymbol{x}}^{\mathrm{b}}\right) \tag{4}$$

If we neglect the influence of the averaging kernel, this equation has the desired shape of Eq. (1), i.e. the sum of the prior value and of a linear function of model-minus-measurement misfits. However, to follow the optimal estimation framework, we still need to be able to develop the product of the gain matrices consistently with Eq. (2), i.e. like (neglecting errors in the observation operators):

$$\mathbf{K} = \widehat{\mathbf{B}}\widehat{\mathbf{H}}^{\mathrm{T}}\breve{\mathbf{H}}^{\mathrm{T}}\left(\breve{\mathbf{H}}\widehat{\mathbf{H}}\widehat{\mathbf{B}}\widehat{\mathbf{H}}^{\mathrm{T}}\breve{\mathbf{H}}^{\mathrm{T}} + \breve{\mathbf{R}}\right)^{-1} \tag{5}$$

In practice, we see that:

$$\widehat{\mathbf{K}}\breve{\mathbf{K}} = \widehat{\mathbf{B}}\widehat{\mathbf{H}}^{\mathrm{T}}\left(\widehat{\mathbf{H}}\widehat{\mathbf{B}}\widehat{\mathbf{H}}^{\mathrm{T}} + \widehat{\mathbf{R}}'\right)^{-1}\breve{\mathbf{B}}\breve{\mathbf{H}}^{\mathrm{T}}\left(\breve{\mathbf{H}}\breve{\mathbf{B}}\breve{\mathbf{H}}^{\mathrm{T}} + \breve{\mathbf{R}}\right)^{-1} \tag{6}$$

Equations (5)–(6) can be made consistent provided

$$\breve{\mathbf{B}} = \widehat{\mathbf{H}}\widehat{\mathbf{B}}\widehat{\mathbf{H}}^{\mathrm{T}} \tag{7}$$

and (using Eq. 7)

$$\left(\widehat{\mathbf{H}}\widehat{\mathbf{B}}\widehat{\mathbf{H}}^{\mathrm{T}} + \widehat{\mathbf{R}}'\right)^{-1}\widehat{\mathbf{H}}\widehat{\mathbf{B}}\widehat{\mathbf{H}}^{\mathrm{T}} = \mathbf{I} \tag{8}$$

Equation (7) simply expresses consistency between the prior error statistics: the uncertainty of the retrieval prior should correspond to the uncertainty of the flux prior projected in the profile space. This condition is not achieved by current satellite retrieval algorithms because they artificially maximize the measurement contribution in

ACPD
15, 11889–11923, 2015

Title Page
Abstract | Introduction
Conclusions | References
Tables | Figures
◂◂ | ▸▸
◂ | ▸
Back | Close
Full Screen / Esc
Printer-friendly Version
Interactive Discussion

the retrievals through the use of very large prior error variances (see Sect. 2.1). However, if enough intermediate variables were saved by the retrieval schemes, it would be possible to reconstruct the retrievals with a different prior error covariance matrix $\breve{\mathbf{B}}$.

Equation (8) can obviously only be satisfied if the retrieval error variances are negligible compared to the flux prior error variances projected in the same space (which would actually relax the previous requirement as well). Typically, the standard deviation of the uncertainty (1σ) in the de-trended columns simulated by free models is not larger than a couple of ppm, at least for broad scale statistics (Chevallier and O'Dell, 2013; Peng et al., 2015), i.e. about the current GOSAT retrieval uncertainty (Oshchepkov et al., 2013). Note that the situation is more favourable when considering TCCON retrievals, because of their better precision.

As a consequence, the effective gain matrix $\widehat{\mathbf{K}}\breve{\mathbf{K}}$ significantly differs from the optimal one for GOSAT, resulting in a wrong balance between prior flux information and measured radiances. Overall, $\breve{\mathbf{K}}$ pulls too much towards the measured radiances and $\widehat{\mathbf{K}}$ pulls too much towards the prior. This suboptimality very likely flaws the 4-D information flow from the radiance measurements to the surface flux estimates. Further, the sub-optimality of $\breve{\mathbf{K}}$ also affects the retrieval averaging kernel that is part of $\widehat{\mathbf{H}}'$, meaning that the model-data- misfits in Eq. (4) are not computed correctly, for instance because the retrieval averaging kernel would not peak low enough in the vertical.

The situation complicates even further if we account for the facts that inversion systems assimilate the retrieved profiles as vertical integrals (because XCO_2 is less sensitive to vertical transport model errors than the CO_2 profile), that these vertical integrals are empirically bias-corrected (thereby implicitly re-introducing $\breve{x}^b$ that had been neutralised by the use of averaging kernels, in the equations) and that $\breve{\mathbf{H}}$ and $\widehat{\mathbf{H}}$ are imperfect operators, the uncertainty of which should be reported in $\breve{\mathbf{R}}$, following Eq. (5). The need to report all observation operator uncertainties in $\breve{\mathbf{R}}$ means that retrieval configuration should in principle be tailored to the retrieval end-application, i.e. to the precision of the observation operator that is used in this end-application. For flux inversion, the transport model uncertainty in XCO_2 space is about 0.5 ppm (1σ, Houweling et al., 2010). When optimizing parameters of a flux model rather than for the flux themselves (in Carbon Cycle Data Assimilation Systems, Rayner et al., 2005), the uncertainty of the flux model equations has also to be reported in $\check{\mathbf{R}}$: when projected in the space of XCO_2, they are comparable to transport model uncertainties (Kuppel et al., 2013).

4 Practical aspects

Given the particular concerns raised about the optimality of XCO_2 retrievals themselves in the previous section, we now focus on one specific retrieval product, ACOS-GOSAT, in order to look for some practical evidence of this sub-optimality.

4.1 Mean differences

Figure 1 shows the mean bias-corrected retrievals $XCO_2^{a,\,c}$ and the mean corresponding posterior XCO_2 field of the MACC inversion over the June 2009–May 2013 period per 3.75° × 1.9° grid cell. All retrievals are used, provided they are found good by the ACOS standard quality control. The data density (Fig. 2b) follows the frequency of favourable retrieval conditions: more sunlight in the Tropics, less cloud over desert areas or over subsidence ocean regions. The long-tern mean of the retrieval-minus-model differences (Fig. 2a) is usually about the ppm, i.e. not much less than the variability of the mean XCO_2 field (Fig. 1). Interestingly, it appears to be organized spatially. Over land, large positive values (> 0.5 ppm, ACOS-GOSAT being larger) are seen over boreal forests, over most of South America, over grassland/cropland regions in Central Africa and over the West coast of the USA. Negative values occur over most of the other lands, with smaller values (up to ∼ −1 ppm) mostly over South and East Asia. Over the oceans, values are mostly positive north of 30° N and south of 10° S, and negative in between. Both errors in ACOS-GOSAT and errors in the model simulations contribute to these differences, which complicates the interpretation of Fig. 2a. For instance, the

ACPD
15, 11889–11923, 2015

On the optimality of satellite-based CO_2 atmospheric inversions

F. Chevallier

zonal structure of the differences over the oceans could well be caused by the model, either because of too few surface air-sample sites in the Tropics or because the LMDZ transport model would not represent the inter-hemispheric exchange well enough (Patra et al., 2011). Alternatively, misrepresented clouds around the convergence zones could also induce them in the retrievals. Some of the patterns of Fig. 2a are similar to the surface cover, like the gradient between the Sahel and the African savannahs, or the one between the equatorial Atlantic and the African savannahs, while we expect the true XCO_2 fields to be first driven by large-scale horizontal advection (Keppel-Aleks et al., 2011). The main local spatial gradients in the mean differences are also seen on monthly means despite less data density (Fig. 3). They mostly reflect the retrieval gradients (Fig. 1a), because the model XCO_2 simulation is spatially smoother (Fig. 1b), even though it uses the retrieval averaging kernels (that change from scene to scene as a function, among other factors, of surface conditions) and even though it is sampled like the retrievals (i.e. with a spatially heterogeneous data density, also varying as a function, among other things, of surface conditions).

The jump of the long-term mean difference from the African savannahs to Sahel or equatorial Atlantic (while there is no jump between subtropical Atlantic and Western Sahara for instance) mostly corresponds to data from March (Fig. 3a), at the end of the savannah burning season (e.g. van der Werf et al., 2010). The model shows elevated values (Fig. 1b), but much less than the retrievals (Fig. 1a). If the model was underestimating the intensity of the fire, we would expect the mean difference to take the shape of a plume, i.e. to spread downstream the source region, but this is not the case. This suggests that the retrievals are affected by systematic errors over this region. Similarly, we note a surprising discontinuity of the mean difference on the north-western coast of the US in Fig. 2a.

The positive differences of Fig. 2a in Eurasia notably follow the boreal forests, while negative values are found over the neighbouring regions of sparse tundra vegetation north of Siberia, or those of grassland/cropland south of them. The same remark applies to North America. The link with boreal forests is less obvious when looking at one

ACPD
15, 11889–11923, 2015

isolated year because of the relatively small number of retrievals in these regions (not shown). The misfit pattern in Siberia and in North America contains many values larger than 1 ppm corresponding to relatively large retrieved XCO_2 (Fig. 1a). These large values are all the more surprising that retrievals in these high latitudes are obtained during the growing season and that boreal forests in Eurasia are identified as large carbon sinks by bottom-up inventories (Pan et al., 2011; Dolman et al., 2012). By comparison, we can look at agricultural regions, where the model could miss gradients during crop growth, both because the MACC inversion prior fluxes do not explicitly represent agricultural practices and because the location of the assimilated surface air-sample measurements only provides rough information about crop fluxes: the differences are marginal (−0.1 ppm on average, whether we compute the mean at the global scale or only for latitudes above 40° N) for retrievals located in crop regions, as identified by the high-resolution land cover map of ESA's Land Cover Climate Change Initiative project (http://www.esa-landcover-cci.org/). In the Corn Belt, the intensively agricultural region in the Midwest of the USA, differences are negative, but they are much smaller in absolute value (the differences are larger than −0.4 ppm) than over the boreal forests, and the Corn Belt boundaries do not sharply appear, in particular on its eastern side. The Corn Belt does not particularly appear in monthly means either (e.g., Fig. 3b). These elements suggest that the long-term mean differences over boreal forests come from a retrieval artifact rather than from the MACC inversion product.

From a radiative transfer point of view, boreal forests are covered with needle-leaved trees with low albedo in the strong CO_2 spectral band of GOSAT near 2.1 µm (Fig. 4): these low values hamper the XCO_2 retrieval. O'Dell et al. (2012) already showed that large positive biases can occur for needle-leaved evergreen forests, with the retrieval exchanging surface albedo for very thin cloud or aerosol. Extreme cases are filtered out by the ACOS-GOSAT quality control, but Fig. 2a suggests that the remaining retrievals over boreal forests, including the region in Siberia East of 100° E which is dominated by deciduous needle-leaved trees with slightly larger albedos, are still biased. In temperate regions, south of 50° N, the differences for needle-leaf cover (mainly in Southeast USA

ACPD
15, 11889–11923, 2015

On the optimality of satellite-based CO_2 atmospheric inversions

F. Chevallier

and Southeast China) have the opposite sign, but they do not show up distinctly in the difference map like the boreal forests. Tropical forests in South America and in Africa also have low albedo and correspond to negative differences. They are more identifiable in Fig. 2a, but could be explained by an insufficient carbon sink in the model as well as by a retrieval artifact.

4.2 Link to the retrieval increment

We now look at the XCO_2 misfit statistics over land and for the high-gain mode as a function of the size of the retrieval increment to its prior information ($XCO_2^a - XCO_2^b$) in Fig. 5. We look at the misfits of the model to XCO_2^a, to $XCO_2^{a,c}$ and to XCO_2^b, in order to visualize the added value brought by the retrieval process and by the bias correction, successively, on top of the prior estimate. This prior estimate about atmospheric CO_2 has been provided to the retrieval scheme by a data-driven empirical model (Wunch et al., 2011a). In Fig. 5, each bin along the abscissa encompasses a large diversity of times during the four years and a large diversity of locations over the globe, over which the model simulation should be overall more accurate (smaller root mean square error) than XCO_2^b, XCO_2^a and even $XCO_2^{a,c}$ (Chevallier and O'Dell, 2013). Further, we expect the model error to be uncorrelated with the error of XCO_2^b, XCO_2^a and $XCO_2^{a,c}$ so that a smaller standard deviation of the misfits (e.g., using XCO_2^a rather than XCO_2^b) can be interpreted in terms of better precision of the corresponding retrieval quantity.

The mean difference significantly varies with the increment size: starting at 0.7 ppm for the smallest increments it reaches about 2 and −1 ppm, for XCO_2^b and XCO_2^a respectively. As expected, the mean difference is systematically better with XCO_2^a than with XCO_2^b. The bias correction ($XCO_2^{a,c}$) further reduces the mean difference to a small extent.

The standard deviation for XCO_2^b is 1.1 ppm for small increments and smoothly increases to 2 ppm for retrieval increments of size 6 ppm. This trend demonstrates some skill of the retrieval algorithm to characterize the error of XCO_2^b from the GOSAT ra-

ACPD
15, 11889–11923, 2015

diances and to generate a sizeable increment accordingly. By comparison, the model variability for a given increment size over the four years ranges between 3 and 4 ppm (1 σ), the prior variability is about 3 ppm and the retrieval variability ranges between 3 and 7 ppm. The standard deviation that uses XCO_2^a is 1.1 ppm for small increments. It smoothly increases to 4 ppm for retrieval increments of size 6 ppm: it is systematically larger than the standard deviation that uses XCO_2^b (despite a smaller mean difference). The standard deviation that uses $XCO_2^{a,c}$ is also 1.1 ppm for small increments and is also systematically larger than the standard deviation that uses XCO_2^b, but it performs better than XCO_2^a. The worse standard deviation of the misfit of XCO_2^a and $XCO_2^{a,c}$ to the model compared to XCO_2^b cannot be explained by a common lack of variability in the model and in XCO_2^b, because thinning the retrievals (for instance by keeping only one retrieval every nine model grid boxes for a given day) only marginally changes the figure (not shown).

The fact that the standard deviation smoothly increases with increment size suggests that the increment size is systematically overestimated. Figure 6 presents an empirical test where we halve the retrieval increments, without any bias correction: we call $XCO_2^{a,r} = XCO_2^b + (XCO_2^a - XCO_2^b)/2$ the result. The reduction is seen to cancel most of the dependency of the statistics of the observation-minus-model misfits to the increment size: the standard deviation and the mean are then stable around 1.1 and -0.3 ppm, respectively for increments up to 4 ppm without any bias correction. The standard deviation is systematically better than for XCO_2^b, which shows added value brought by the radiance measurements, in contrast to the previous results.

For the medium-gain retrievals (Fig. 7) and for the ocean glint retrievals (Fig. 8), the standard deviation of the misfits using $XCO_2^{a,c}$ is not significantly larger than that using XCO_2^b.

Discussion Paper | Discussion Paper | Discussion Paper | Discussion Paper |
ACPD
15, 11889–11923, 2015
On the optimality of satellite-based CO_2 atmospheric inversions
F. Chevallier

5 Discussion and conclusions

Small uncertainties in aerosols, cirrus cloud or surface albedo are known to heavily affect the quality of the XCO_2 satellite retrievals and to propagate into biases in the fluxes inverted from them, even when the parasite signal in XCO_2 is sub-ppm. This weakness lead the science team of NASA's OCO, a satellite that failed at launch in February 2009, to conclude that the space-based NIR/SWIR measurements of XCO_2 could not be used alone for CO_2 source-sink inversions and that they had to be combined with observations from a reasonable number of surface stations (Miller et al., 2007). However, so much improvement has been obtained in these issues by various institutes during the last few years, that it is sometimes thought that the space-borne XCO_2 retrievals have reached sufficient quality for source-sink inversion. The present paper discusses where we stand in this respect both from general theoretical considerations and from one of the most advanced GOSAT retrieval products.

From the theory, we have shown that a two-step approach to infer the surface fluxes from the GOSAT measured radiances, with CO_2 retrievals as an intermediate product, cannot be optimal. This suboptimality corrupts the 4-D information flow from the radiance measurements to the surface flux estimates. It is amplified by the current retrieval strategy where prior errors are much larger (by an order of magnitude in terms of variances) than the performance of prior CO_2 simulations used in atmospheric inversions. Indeed, the use of averaging kernels makes atmospheric inversion insensitive to the choice of a particular retrieval prior CO_2 profile (Connor et al., 1994) if retrievals are assimilated without any bias correction, but it does not make the retrieval prior error statistics disappear from the inverse modelling equations. The current strategy likely generates retrieval averaging kernels that are inappropriate for atmospheric inversions in their default configurations, with a wrong vertical distribution and an excessive weight towards the measured radiances. Paradoxically, empirical bias correction of the retrievals (e.g., Wunch et al., 2011b) also contributes to the degradation of the 4-D information flow, because it carries the imprint of the retrieval prior and of the retrieval prior error statistics. Direct assimilation of the measured radiances would solve the inconsistency, but would increase the computational burden of atmospheric inversions by several orders of magnitude. Alternatively, we could adapt the inversion systems to the current retrieval configuration by using minimal prior information about the surface fluxes, typically a flat prior flux field, but the result would still over-fit the measured radiances due to the absence of other (compensating) information. We note that the situation is more favourable when assimilating TCCON retrievals, as has been done by Chevallier et al. (2011), or possibly future OCO-2 retrievals, due to better measurement precision than for GOSAT.

We have compared the ACOS-GOSAT retrievals with a transport model simulation constrained by surface air-sample measurements in order to find some evidence of retrieval sub-optimality. Flaws in this transport model and in these inverted surface fluxes necessarily flaw the simulation in many places over the globe and at various times of the year. We therefore carefully selected some of the relatively large discontinuities in the XCO_2 fields that the simulation unlikely generated. We found some evidence of retrieval systematic errors over the dark surfaces of the high-latitude lands and over African savannahs. We note that the mean differences over the African savannahs could be explained by retrieval averaging kernels not peaking low enough in the atmosphere further to the assignment of loose retrieval prior error variances. Biomass burning aerosols that would not be well identified by the retrieval scheme could also play a role. We also found some evidence that the high-gain retrievals over land systematically over-fit the measured radiances, as a consequence of the prior uncertainty overestimation and of an underestimation of the observation uncertainty (as seen by the underlying radiative transfer model). This over-fit is partially compensated by the bias correction. An empirical test indicates that halving the retrieval increments without any posterior bias correction actually cancels the dependency of the statistics of the observation-minus-model misfits to the increment size and makes the standard deviation systematically better than for the retrieval prior XCO_2^b, which shows added value brought by the radiance measurements, in contrast to the previous results. We argue

Discussion Paper | Discussion Paper | Discussion Paper | Discussion Paper |
ACPD
15, 11889–11923, 2015
On the optimality of satellite-based CO_2 atmospheric inversions
F. Chevallier

here that the optimal-estimation retrieval process and, consequently, its posterior bias correction need retuning.

Given the diversity of existing satellite retrieval algorithms, our conclusions cannot be easily extrapolated to other GOSAT retrieval products and even less to XCO_2 retrievals from other instruments, but we note that such mistuning like the one highlighted here is common practice, both because the errors of the retrieval forward model are difficult to characterize and because satellite retrievals are usually explicitly designed to maximize the observation contribution, at the risk of over-fitting radiance and forward model noise. A primary consequence of this mistuning is the usual underestimation of retrieval errors: for instance, O'Dell et al. (2012) recommended inflating this error by a twofold factor for ACOS-GOSAT b2.8. More importantly, our results show that the mistuning generates excessive (unphysical) space–time variations of the retrievals up to $\sim 1\,\%$. This noise level would not matter for short-lived species, but for CO_2 it is enough to significantly degrade the assimilation of the retrievals for flux inversion and may explain some of the inconsistency seen between GOSAT-based top-down results and bottom-up results for CO_2 (Chevallier et al., 2014; Reuter et al., 2014). Therefore, with the current mistuning, we reiterate previous recommendations to take GOSAT-based CO_2 inversion results particularly cautiously. But we also suggest that this situation may dramatically improve by simply retuning the retrieval schemes. Ultimately, internal statistical consistency of the retrievals and of the inversion schemes is needed to establish the credibility of their end product.

Acknowledgements. Some of this work was performed using HPC resources of DSM-CCRT and of CCRT under the allocation t2014012201 made by GENCI (Grand Équipement National de Calcul Intensif). It was co-funded by the European Commission under the EU H2020 Programme (grant agreement No. 630080, MACC III). The ACOS GOSAT data can be obtained from http://co2.jpl.nasa.gov. They were produced by the ACOS/OCO-2 project at the Jet Propulsion Laboratory, California Institute of Technology, using GOSAT observed spectral radiances made available by the GOSAT project. The MACC product can be obtained from http://www.copernicus-atmosphere.eu. The author is very grateful to the many people involved in the surface CO_2 measurements and in the archiving of these data that were kindly made available to him. He also thanks C. O'Dell for many fruitful and stimulating discussions about the topics addressed here.

References

Aben, I., Hasekamp, O., and Hartmann, W.: Uncertainties in the space-based measurements of CO_2 columns due to scattering in the Earth's atmosphere, J. Quant. Spectrosc. Ra., 104, 450–459, 2007.

Basu, S., Guerlet, S., Butz, A., Houweling, S., Hasekamp, O., Aben, I., Krummel, P., Steele, P., Langenfelds, R., Torn, M., Biraud, S., Stephens, B., Andrews, A., and Worthy, D.: Global CO_2 fluxes estimated from GOSAT retrievals of total column CO_2, Atmos. Chem. Phys., 13, 8695–8717, doi:10.5194/acp-13-8695-2013, 2013.

Basu, S., Krol, M., Butz, A., Clerbaux, C., Sawa, Y., Machida, T., Matsueda, H., Frankenberg, C., Hasekamp, O. P., and Aben, I.: The seasonal variation of the CO_2 flux over Tropical Asia estimated from GOSAT, CONTRAIL, and IASI, Geophys. Res. Lett., 41, 1809–1815, doi:10.1002/2013GL059105, 2014.

Boesch, H., Toon, G. C., Sen, B., Washenfelder, R. A., Wennberg, P. O., Buchwitz, M., de Beek, R., Burrows, J. P., Crisp, D., Christi, M., Connor, B. J., Natraj, V., and Yung, Y. L.: Space-based near-infrared CO_2 measurements: testing the Orbiting Carbon Observatory retrieval algorithm and validation concept using SCIAMACHY observations over Park Falls, Wisconsin, J. Geophys. Res.-Atmos., 111, D23302, doi:10.1029/2006JD007080, 2006.

Buchwitz, M., de Beek, R., Burrows, J. P., Bovensmann, H., Warneke, T., Notholt, J., Meirink, J. F., Goede, A. P. H., Bergamaschi, P., Körner, S., Heimann, M., and Schulz, A.: Atmospheric methane and carbon dioxide from SCIAMACHY satellite data: initial comparison with chemistry and transport models, Atmos. Chem. Phys., 5, 941–962, doi:10.5194/acp-5-941-2005, 2005.

Chédin, A., Serrar, S., Scott, N. A., Crevoisier, C., and Armante, R.: First global measurement of midtropospheric CO_2 from NOAA polar satellites: tropical zone, J. Geophys. Res., 108, 4581, doi:10.1029/2003JD003439, 2003.

Chevallier, F.: Impact of correlated observation errors on inverted CO_2 surface fluxes from OCO measurements, Geophys. Res. Lett., 34, L24804, doi:10.1029/2007GL030463, 2007.

ACPD
15, 11889–11923, 2015

Chevallier, F. and O'Dell, C. W.: Error statistics of Bayesian CO_2 flux inversion schemes as seen from GOSAT, Geophys. Res. Lett., 40, 1252–1256, doi:10.1002/grl.50228, 2013.

Chevallier, F., Fisher, M., Peylin, P., Serrar, S., Bousquet, P., Bréon, F.-M., Chédin, A., and Ciais, P.: Inferring CO_2 sources and sinks from satellite observations: method and application to TOVS data, J. Geophys. Res., 110, D24309, doi:10.1029/2005JD006390, 2005.

Chevallier, F., Bréon, F.-M., and Rayner, P. J.: The contribution of the Orbiting Carbon Observatory to the estimation of CO_2 sources and sinks: theoretical study in a variational data assimilation framework, J. Geophys. Res., 112, D09307, doi:10.1029/2006JD007375, 2007.

Chevallier, F., Ciais, P., Conway, T. J., Aalto, T., Anderson, B. E., Bousquet, P., Brunke, E. G., Ciattaglia, L., Esaki, Y., Fröhlich, M., Gomez, A., Gomez-Pelaez, A. J., Haszpra, L., Krummel, P. B., Langenfelds, R. L., Leuenberger, M., Machida, T., Maignan, F., Matsueda, H., Morgui, J. A., Mukai, H., Nakazawa, T., Peylin, P., Ramonet, M., Rivier, L., Sawa, Y., Schmidt, M., Steele, L. P., Vay, S. A., Vermeulen, A. T., Wofsy, S., and Worthy, D.: CO_2 surface fluxes at grid point scale estimated from a global 21 year reanalysis of atmospheric measurements, J. Geophys. Res., 115, D21307, doi:10.1029/2010JD013887, 2010.

Chevallier, F., Deutscher, N., Conway, T. J., Ciais, P., Ciattaglia, L., Dohe, S., Fröhlich, M., Gomez-Pelaez, A. J., Griffith, D., Hase, F., Haszpra, L., Krummel, P., Kyrö, E., Labuschagne, C., Langenfelds, R., Machida, T., Maignan, F., Matsueda, H., Morino, I., Notholt, J., Ramonet, M., Sawa, Y., Schmidt, M., Sherlock, V., Steele, P., Strong, K., Sussmann, R., Wennberg, P., Wofsy, S., Worthy, D., Wunch, D., and Zimnoch, M.: Global CO_2 fluxes inferred from surface air-sample measurements and from TCCON retrievals of the CO_2 total column, Geophys. Res. Lett., 38, L24810, doi:10.1029/2011GL049899, 2011.

Chevallier, F., Palmer, P. I., Feng, L., Boesch, H., O'Dell, C. W., and Bousquet, P.: Towards robust and consistent regional CO_2 flux estimates from in situ and space-borne measurements of atmospheric CO_2, Geophys. Res. Lett., 41, 1065–1070, doi:10.1002/2013GL058772, 2014.

Connor, B. J., Siskind, D. E., Tsou, J. J., Parrish, A., and Remsberg, E. E.: Ground-based microwave observations of ozone in the upper stratosphere and mesosphere, J. Geophys. Res., 99, 16757–16770, 1994.

Connor, B. J., Boesch, H., Toon, G., Sen, B., Miller, C., and Crisp, D.: Orbiting Carbon Observatory: inverse method and prospective error analysis, J. Geophys. Res.-Atmos., 113, D05305, doi:10.1029/2006JD008336, 2008.

ACPD
15, 11889–11923, 2015

Crisp, D., Fisher, B. M., O'Dell, C., Frankenberg, C., Basilio, R., Bösch, H., Brown, L. R., Castano, R., Connor, B., Deutscher, N. M., Eldering, A., Griffith, D., Gunson, M., Kuze, A., Mandrake, L., McDuffie, J., Messerschmidt, J., Miller, C. E., Morino, I., Natraj, V., Notholt, J., O'Brien, D. M., Oyafuso, F., Polonsky, I., Robinson, J., Salawitch, R., Sherlock, V., Smyth, M., Suto, H., Taylor, T. E., Thompson, D. R., Wennberg, P. O., Wunch, D., and Yung, Y. L.: The ACOS CO_2 retrieval algorithm – Part II: Global X_{CO_2} data characterization, Atmos. Meas. Tech., 5, 687–707, doi:10.5194/amt-5-687-2012, 2012.

Dolman, A. J., Shvidenko, A., Schepaschenko, D., Ciais, P., Tchebakova, N., Chen, T., van der Molen, M. K., Belelli Marchesini, L., Maximov, T. C., Maksyutov, S., and Schulze, E.-D.: An estimate of the terrestrial carbon budget of Russia using inventory-based, eddy covariance and inversion methods, Biogeosciences, 9, 5323–5340, doi:10.5194/bg-9-5323-2012, 2012.

Global Climate Observing System (GCOS): Systematic observation requirements for satellite-based products for climate, Supplemental details to the satellite-based component of the "Implementation Plan for the Global Observing System for Climate in Support of the UNFCCC (2010 update)", Prepared by World Meteorological Organization (WMO), Doc.: GCOS 154, Intergovernmental Oceanographic Commission, United Nations Environment Programme (UNEP), International Council for Science, 2010.

Guerlet, S., Basu, S., Butz, A., Krol, M. C., Hahne, P., Houweling, S., Hasekamp, O. P., and Aben, I.: Reduced carbon uptake during the 2010 Northern Hemisphere summer as observed from GOSAT, Geophys. Res. Lett., 40, 2378–2383, doi:10.1002/grl.50402, 2013a.

Guerlet, S., Butz, A., Schepers, D., Basu, S., Hasekamp, O. P., Kuze, A., Yokota, T., Blavier, J.-F., Deutscher, N. M., Griffith, D. W. T., Hase, F., Kyrö, E., Morino, I., Sherlock, V., Sussmann, R., Galli, A., and Aben, I.: Impact of aerosol and thin cirrus on retrieving and validating XCO_2 from GOSAT shortwave infrared measurements, J. Geophys. Res.-Atmos., 118, 4887–4905, doi:10.1002/jgrd.50332, 2013b.

Hourdin, F., Musat, I., Bony, S., Braconnot, P., Codron, F., Dufresne, J. L., Fairhead, L., Filiberti, M. A., Friedlingstein, P., Grandpeix, J. Y., Krinner, G., Levan, P., Li, Z. X., and Lott, F.: The LMDZ4 general circulation model: climate performance and sensitivity to parametrized physics with emphasis on tropical convection, Clim. Dynam., 27, 787–813, doi:10.1007/s00382-006-0158-0, 2006.

Houweling, S., Aben, I., Breon, F.-M., Chevallier, F., Deutscher, N., Engelen, R., Gerbig, C., Griffith, D., Hungershoefer, K., Macatangay, R., Marshall, J., Notholt, J., Peters, W., and

Serrar, S.: The importance of transport model uncertainties for the estimation of CO_2 sources and sinks using satellite measurements, Atmos. Chem. Phys., 10, 9981–9992, doi:10.5194/acp-10-9981-2010, 2010.

Ingmann, P.: A-SCOPE, Advanced Space Carbon and Climate Observation of Planet Earth, Report of Assessment, SP-1313/1, ESA Communication Product Office, Noordwijk, the Netherlands, 2009.

Keppel-Aleks, G., Wennberg, P. O., and Schneider, T.: Sources of variations in total column carbon dioxide, Atmos. Chem. Phys., 11, 3581–3593, doi:10.5194/acp-11-3581-2011, 2011.

Kuppel, S., Chevallier, F., and Peylin, P.: Quantifying the model structural error in carbon cycle data assimilation systems, Geosci. Model Dev., 6, 45–55, doi:10.5194/gmd-6-45-2013, 2013.

Maksyutov, S., Kadygrov, N., Nakatsuka, Y., Patra, P. K., Nakazawa, T., Yokota, T., and Inoue, G.: Projected impact of the GOSAT observations on regional CO_2 flux estimations as a function of total retrieval error, J. Remote Sens. Soc. Jpn., 28, 190–197, 2008.

Miller, C. E., Crisp, D., DeCola, P. L., Olsen, S. C., Randerson, J. T., Michalak, A. M., Alkhaled, A., Rayner, P., Jacob, D. J., Suntharalingam, P., Jones, D. B. A., Denning, A. S., Nicholls, M. E., Doney, S. C., Pawson, S., Boesch, H., Connor, B. J., Fung, I. Y., O'Brien, D., Salawitch, R. J., Sander, S. P., Sen, B., Tans, P., Toon, G. C., Wennberg, P. O., Wofsy, S. C., Yung, Y. L., and Law, R. M.: Precision requirements for space-based $X\mathrm{CO}_2$ data, J. Geophys. Res., 112, D10314, doi:10.1029/2006JD007659, 2007.

Nguyen, H., Osterman, G., Wunch, D., O'Dell, C., Mandrake, L., Wennberg, P., Fisher, B., and Castano, R.: A method for colocating satellite X_{CO_2} data to ground-based data and its application to ACOS-GOSAT and TCCON, Atmos. Meas. Tech., 7, 2631–2644, doi:10.5194/amt-7-2631-2014, 2014.

O'Dell, C. W., Connor, B., Bösch, H., O'Brien, D., Frankenberg, C., Castano, R., Christi, M., Eldering, D., Fisher, B., Gunson, M., McDuffie, J., Miller, C. E., Natraj, V., Oyafuso, F., Polonsky, I., Smyth, M., Taylor, T., Toon, G. C., Wennberg, P. O., and Wunch, D.: The ACOS CO_2 retrieval algorithm – Part 1: Description and validation against synthetic observations, Atmos. Meas. Tech., 5, 99–121, doi:10.5194/amt-5-99-2012, 2012.

Oshchepkov, S., Bril, A., Yokota, T., Wennberg, P. O., Deutscher, N. M., Wunch, D., Toon, G. C., Yoshida, Y., O'Dell, C. W., Crisp, D., Miller, C. E., Frankenberg, C., Butz, A., Aben, I., Guerlet, S., Hasekamp, O., Boesch, H., Cogan, A., Parker, R., Griffith, D., Macatangay, R., Notholt, J., Sussmann, R., Rettinger, M., Sherlock, V., Robinson, J., Kyrö, E., Heikki-

ACPD
15, 11889–11923, 2015

On the optimality of satellite-based CO_2 atmospheric inversions

F. Chevallier

nen, P., Feist, D. G., Morino, I., Kadygrov, N., Belikov, D., Maksyutov, S., Matsunaga, T., Uchino, O., and Watanabe, H.: Effects of atmospheric light scattering on spectroscopic observations of greenhouse gases from space. Part 2: Algorithm intercomparison in the GOSAT data processing for CO_2 retrievals over TCCON sites, J. Geophys. Res., 118, 1493–1512, doi:10.1002/jgrd.50146, 2013.

Osterman, G., Eldering, A., Avis, C., O'Dell, C., Martinez, E., Crisp, D., Frankenberg, C., and Frankenberg, B.: ACOS Level 2 Standard Product Data User's Guide v3.4, Revision Date: Revision B, 3 October 2013, available at: https://co2.jpl.nasa.gov/static/docs/v3.4_DataUsersGuide-RevB_131028.pdf (last access: 20 April 2015), 2013.

Pan, Y., Birdsey, R. A., Fang, J., Houghton, R., Kauppi, P. E., Kurz, W. A., Phillips, O. L., Shvidenko, A., Lewis, S. L., Canadell, J. G., Ciais, P., Jackson, J. B., Pacala, S., McGuire, A. D., Piao, S., Rautiainen, A., Sitch, S., and Hayes, D.: A large and persistent carbon sink in the world's forests, Science, 333, 988–993, 2011.

Patra, P. K., Houweling, S., Krol, M., Bousquet, P., Belikov, D., Bergmann, D., Bian, H., Cameron-Smith, P., Chipperfield, M. P., Corbin, K., Fortems-Cheiney, A., Fraser, A., Gloor, E., Hess, P., Ito, A., Kawa, S. R., Law, R. M., Loh, Z., Maksyutov, S., Meng, L., Palmer, P. I., Prinn, R. G., Rigby, M., Saito, R., and Wilson, C.: TransCom model simulations of CH_4 and related species: linking transport, surface flux and chemical loss with CH_4 variability in the troposphere and lower stratosphere, Atmos. Chem. Phys., 11, 12813–12837, doi:10.5194/acp-11-12813-2011, 2011.

Peng, S., Ciais, P., Chevallier, F., Peylin, P., Cadule, P., Sitch, S., Piao, S., Ahlström, A., Huntingford, C., Levy, P., Li, X., Liu, Y., Lomas, M., Poulter, B., Viovy, N., Wang, T., Wang, X., Zaehle, S., Zeng, N., Zhao, F., and Zhao, H.: Benchmarking the seasonal cycle of CO_2 fluxes simulated by terrestrial ecosystem models, Global Biogeochem. Cy., 29, 46–64, doi:10.1002/2014GB004931, 2015.

Peylin, P., Law, R. M., Gurney, K. R., Chevallier, F., Jacobson, A. R., Maki, T., Niwa, Y., Patra, P. K., Peters, W., Rayner, P. J., Rödenbeck, C., van der Laan-Luijkx, I. T., and Zhang, X.: Global atmospheric carbon budget: results from an ensemble of atmospheric CO_2 inversions, Biogeosciences, 10, 6699–6720, doi:10.5194/bg-10-6699-2013, 2013.

Rayner, P., Scholze, M., Knorr, W., Kaminski, T., Giering, R., and Widmann, H.: Two decades of terrestrial Carbon fluxes from a Carbon Cycle Data Assimilation System (CCDAS), Global Biogeochem. Cy., 19, GB2026, doi:10.1029/2004GB002254, 2005.

ACPD
15, 11889–11923, 2015

On the optimality of satellite-based CO_2 atmospheric inversions

F. Chevallier

Reuter, M., Buchwitz, M., Schneising, O., Heymann, J., Bovensmann, H., and Burrows, J. P.: A method for improved SCIAMACHY CO_2 retrieval in the presence of optically thin clouds, Atmos. Meas. Tech., 3, 209–232, doi:10.5194/amt-3-209-2010, 2010.

Reuter, M., Buchwitz, M., Hilker, M., Heymann, J., Schneising, O., Pillai, D., Bovensmann, H., Burrows, J. P., Bösch, H., Parker, R., Butz, A., Hasekamp, O., O'Dell, C. W., Yoshida, Y., Gerbig, C., Nehrkorn, T., Deutscher, N. M., Warneke, T., Notholt, J., Hase, F., Kivi, R., Sussmann, R., Machida, T., Matsueda, H., and Sawa, Y.: Satellite-inferred European carbon sink larger than expected, Atmos. Chem. Phys., 14, 13739–13753, doi:10.5194/acp-14-13739-2014, 2014.

Rodgers, C. D.: Inverse Methods for Atmospheric Sounding: Theory and Practice, World Scientific Publishing Co. Ltd., London, 2000.

van der Werf, G. R., Randerson, J. T., Giglio, L., Collatz, G. J., Mu, M., Kasibhatla, P. S., Morton, D. C., DeFries, R. S., Jin, Y., and van Leeuwen, T. T.: Global fire emissions and the contribution of deforestation, savanna, forest, agricultural, and peat fires (1997–2009), Atmos. Chem. Phys., 10, 11707–11735, doi:10.5194/acp-10-11707-2010, 2010.

Wunch, D., Toon, G. C., Blavier, J.-F. L., Washenfelder, R. A., Notholt, J., Connor, B. J., Griffith, D. W. T., Sherlock, V., and Wennberg, P. O.: The total carbon column observing network, Philos. T. Roy. Soc. A, 369, 2087–2112, doi:10.1098/rsta.2010.0240, 2011a.

Wunch, D., Wennberg, P. O., Toon, G. C., Connor, B. J., Fisher, B., Osterman, G. B., Frankenberg, C., Mandrake, L., O'Dell, C., Ahonen, P., Biraud, S. C., Castano, R., Cressie, N., Crisp, D., Deutscher, N. M., Eldering, A., Fisher, M. L., Griffith, D. W. T., Gunson, M., Heikkinen, P., Keppel-Aleks, G., Kyrö, E., Lindenmaier, R., Macatangay, R., Mendonca, J., Messerschmidt, J., Miller, C. E., Morino, I., Notholt, J., Oyafuso, F. A., Rettinger, M., Robinson, J., Roehl, C. M., Salawitch, R. J., Sherlock, V., Strong, K., Sussmann, R., Tanaka, T., Thompson, D. R., Uchino, O., Warneke, T., and Wofsy, S. C.: A method for evaluating bias in global measurements of CO_2 total columns from space, Atmos. Chem. Phys., 11, 12317–12337, doi:10.5194/acp-11-12317-2011, 2011b.

ACPD

15, 11889–11923, 2015

On the optimality of satellite-based CO_2 atmospheric inversions

F. Chevallier

Table 1. List of the continuous sites used in the MACC CO_2 inversion v13r1 together with the period of coverage (defined as the period between the first sample and the last one), and the data source. Each station is identified by the name of the place, the corresponding country (abbreviated) and the code used in the corresponding database.

Locality (indentifier)	Period	Source
Alert, Nunavut, CA (ALT)	1988–2012	WDCGG/EC
Amsterdam Island, FR (AMS)	1981–2011	LSCE
Argyle, Maine, US (AMT)	2003–2011	NOAA/ESRL
Anmyeon-do, KR (AMY)	1999–2012	WDCGG/KMA
Barrow, Alaska, US (BRW)	1979–2013	NOAA/ESRL
Candle Lake, CA (CDL)	2002–2012	WDCGG/EC
Monte Cimone, IT (CMN)	1996–2010	WDCGG/IAFMS
Cape Ochi-ishi, JP (COI)	1995–2002	WDCGG/NIES
Cape Point, SA (CPT)	1993–2013	WDCGG/SAWS
Egbert, CA (EGB)	2005–2012	WDCGG/EC
East Trout Lake, CA (ETL)	2005–2012	WDCGG/EC
Frasedale, CA (FSD)	1990–2012	WDCGG/EC
Hateruma, JP (HAT)	1993–2002	WDCGG/NIES
Hegyhatsal tower, 115 m level, HU (HUN0115)	1994–2013	WDCGG/HMS
Tenerife, Canary Islands, ES (IZO)	1984–2013	WDCGG/AEMET
Jubany, Antartica, AR (JBN)	1994–2009	WDCGG/ISAC IAA
Jungfraujoch, CH (JFJ)	2004–2013	WDCGG/Univ. Of Bern
K-puszta, HU (KPS)	1981–1999	WDCGG/HMS
Park Falls, Wisconsin, US (LEF)	2003–2011	NOAA/ESRL
Mace Head, County Galway, IE (MHD)	1992–2012	LSCE
Mauna Loa, Hawaii, US (MLO)	1979–2013	NOAA/ESRL
Minamitorishima, JP (MNM)	1993–2013	WDCGG/JMA
Pallas-Sammaltunturi, GAW Station, FI (PAL)	1999–2013	WDCGG/FMI
Plateau Rosa, IT (PRS)	2000–2013	WDCGG/CESI RICERCA
Puy de Dome, FR (PUY)	2000–2010	LSCE
Ryori, JP (RYO)	1987–2013	WDCGG/JMA
Tutuila, American Samoa (SMO)	1979–2013	NOAA/ESRL
Sonnblick, AU (SNB)	1999–2013	WDCGG/EEA
South Pole, Antarctica, US (SPO)	1979–2013	NOAA/ESRL
Tsukuba tower, 200 m level, JP (TKB)	1986–2000	WDCGG/MRI
Westerland, DE (WES)	1979–2013	WDCGG/UBA
Moody, Texas, US (WKT)	2003–2011	NOAAA/ESRL
Yonagunijima, JP (YON)	1997–2013	WDCGG/JMA

ACPD
15, 11889–11923, 2015

Table 2. Same as Table 1 but for the flask-sampling sites.

Locality (indentifier)	Period	Source
Alert, Nunavut, CA (ALT)	1985–2013	NOAA/ESRL
Amsterdam Island, FR (AMS)	1979–1990	NOAA/ESRL
Amsterdam Island, FR (AMS)	2003–2013	LSCE
Ascension Island, GB (ASC)	1979–2013	NOAA/ESRL
Assekrem, DZ (ASK)	1995–2013	NOAA/ESRL
St. Croix, Virgin Islands, USA (AVI)	1979–1990	NOAA/ESRL
Terceira Island, Azores, PT (AZR)	1979–2013	NOAA/ESRL
Baltic Sea, PL (BAL)	1992–2011	NOAA/ESRL
Bering Island, RU (BER)	1986–1994	WDCGG/MGO
Begur, ES (BGU)	2000–2013	LSCE/IC• 3
Baring Head, NZ (BHD)	1999–2013	NOAA/ESRL
Baring Head, NZ (BHD)	1979–2011	WDCGG/NIWA
Bukit Kototabang, ID (BKT)	2004–2013	NOAA/ESRL
St. Davids Head, Bermuda, GB (BME)	1989–2009	NOAA/ESRL
Tudor Hill, Bermuda, GB (BMW)	1989–2013	NOAA/ESRL
Barrow, Alaska, US (BRW)	1979–2013	NOAA/ESRL
Portsall, FR (BZH)	1998–2001	CarboEurope/LSCE
Cold Bay, Alaska, US (CBA)	1979–2013	NOAA/ESRL
Cape Ferguson, AU (CFA)	1991–2013	WDCGG/CSIRO
Cape Grim, Tasmania, AU (CGO)	1984–2013	NOAA/ESRL
Christmas Island, Republic of Kiribati (CHR)	1984–2013	NOAA/ESRL
Cape Meares, Oregon, US (CMO)	1982–1998	NOAA/ESRL
Crozet Island, FR (CRZ)	1991–2013	NOAA/ESRL
Cape St. James, CA (CSJ)	1979–1992	WDCGG/EC
Casey Station, AU (CYA)	1996–2013	WDCGG/CSIRO
Drake Passage (DRP)	2003–2013	NOAA/ESRL
Easter Island, CL (EIC)	1994–2013	NOAA/ESRL
Estevan Point, British Columbia, CA (ESP)	1992–2012	WDCGG/EC
Estevan Point, British Columbia, CA (ESP)	1993–2001	WDCGG/CSIRO
Finokalia, Crete, GR (FIK)	1999–2013	LSCE
Mariana Islands, Guam (GMI)	1979–2013	NOAA/ESRL
Dwejra Point, Gozo, MT (GOZ)	1993–1999	NOAA/ESRL
Halley Station, Antarctica, GB (HBA)	1983–2013	NOAA/ESRL
Hohenpeissenberg, DE (HPB)	2006–2013	NOAA/ESRL
Hegyhatsal, HU (HUN)	1993–2013	NOAA/ESRL
Storhofdi, Vestmannaeyjar, IS (ICE)	1992–2013	NOAA/ESRL
Grifton, North Carolina, US (ITN)	1992–1999	WDCGG/ESRL
Tenerife, Canary Islands, ES (IZO)	1991–2013	NOAA/ESRL
Key Biscayne, Florida, US (KEY)	1979–2013	NOAA/ESRL
Kotelny Island, RU (KOT)	1986–1993	WDCGG/MGO
Cape Kumukahi, Hawaii, US (KUM)	1979–2013	NOAA/ESRL
Sary Taukum, KZ (KZD)	1997–2009	NOAA/ESRL
Plateau Assy, KZ (KZM)	1997–2009	NOAA/ESRL
Lulin, TW (LLN)	2006–2013	NOAA/ESRL
Lampedusa, IT (LMP)	2006–2013	NOAA/ESRL
Ile grande, FR (LPO)	2004–2013	LSCE
Mawson, AU (MAA)	1990–2013	WDCGG/CSIRO
Mould Bay, Nunavut, CA (MBC)	1980–1997	NOAA/ESRL
Mace Head, County Galway, IE (MHD)	1991–2013	NOAA/ESRL
Mace Head, County Galway, IE (MHD)	1996–2013	LSCE
Sand Island, Midway, US (MID)	1985–2013	NOAA/ESRL
Mt. Kenya, KE (MKN)	2003–2011	NOAA/ESRL
Mauna Loa, Hawaii, US (MLO)	1979–2013	NOAA/ESRL
Macquarie Island, AU (MQA)	1990–2013	WDCGG/CSIRO
Gobabeb, NA (NMB)	1997–2013	NOAA/ESRL
Niwot Ridge, Colorado, US (NWR)	1979–2013	NOAA/ESRL
Olympic Peninsula, WA, USA (OPW)	1984–1990	NOAA/ESRL
Ochsenkopf, DE (OXK)	2003–2013	NOAA/ESRL
Pallas-Sammaltunturi, GAW Station, FI (PAL)	2001–2013	NOAA/ESRL

ACPD
15, 11889–11923, 2015

Table 2. Continued.

Locality (indentifier)	Period	Source
Pic du Midi, FR (PDM)	2001–2013	LSCE
Pacific Ocean, 0N (POC000)	1987–2011	NOAA/ESRL
Pacific Ocean, 5N (POCN05)	1987–2011	NOAA/ESRL
Pacific Ocean, 10N (POCN10)	1987–2011	NOAA/ESRL
Pacific Ocean, 15N (POCN15)	1987–2011	NOAA/ESRL
Pacific Ocean, 20N (POCN20)	1987–2011	NOAA/ESRL
Pacific Ocean, 25N (POCN25)	1987–2011	NOAA/ESRL
Pacific Ocean, 30N (POCN30)	1987–2011	NOAA/ESRL
Pacific Ocean, 5S (POCS05)	1987–2011	NOAA/ESRL
Pacific Ocean, 10S (POCS10)	1987–2011	NOAA/ESRL
Pacific Ocean, 15S (POCS15)	1987–2011	NOAA/ESRL
Pacific Ocean, 20S (POCS20)	1987–2011	NOAA/ESRL
Pacific Ocean, 25S (POCS25)	1987–2011	NOAA/ESRL
Pacific Ocean, 30S (POCS30)	1987–2011	NOAA/ESRL
Pacific Ocean, 35S (POCS35)	1987–2011	NOAA/ESRL
Palmer Station, Antarctica, US (PSA)	1979–2013	NOAA/ESRL
Point Arena, California, US (PTA)	1999–2011	NOAA/ESRL
Puy de Dome, FR (PUY)	2001–2013	LSCE
Ragged Point, BB (RPB)	1987–2013	NOAA/ESRL
South China Sea, 3N (SCSN03)	1991–1998	NOAA/ESRL
South China Sea, 6N (SCSN06)	1991–1998	NOAA/ESRL
South China Sea, 9N (SCSN09)	1991–1998	NOAA/ESRL
South China Sea, 12N (SCSN12)	1991–1998	NOAA/ESRL
South China Sea, 15N (SCSN15)	1991–1998	NOAA/ESRL
South China Sea, 18N (SCSN18)	1991–1998	NOAA/ESRL
South China Sea, 21N (SCSN21)	1991–1998	NOAA/ESRL
Mahe Island, SC (SEY)	1980–2013	NOAA/ESRL
Southern Great Plains, Oklahoma, US (SGP)	2002–2013	NOAA/ESRL
Shemya Island, Alaska, US (SHM)	1985–2013	NOAA/ESRL
Ship between Ishigaki Island and Hateruma Island, JP (SIH)	1993–2005	WDCGG/Tohoku University
Shetland, Scotland, GB (SIS)	1992–2003	WDCGG/CSIRO
Tutuila, American Samoa (SMO)	1979–2013	NOAA/ESRL
South Pole, Antarctica, US (SPO)	1979–2013	NOAA/ESRL
Ocean Station M, NO (STM)	1980–2009	NOAA/ESRL
Summit, GL (SUM)	1997–2013	NOAA/ESRL
Syowa Station, Antarctica, JP (SYO)	1986–2013	NOAA/ESRL
Tae-ahn Peninsula, KR (TAP)	1991–2013	NOAA/ESRL
Tierra Del Fuego, Ushuaia, AR (TDF)	1994–2013	NOAA/ESRL
Trinidad Head, California, US (THD)	2002–2013	NOAA/ESRL
Tromelin Island, F (TRM)	1998–2007	LSCE
Wendover, Utah, US (UTA)	1993–2013	NOAA/ESRL
Ulaan Uul, MN (UUM)	1992–2013	NOAA/ESRL
Sede Boker, Negev Desert, IL (WIS)	1995–2013	NOAA/ESRL
Sable Island, CA (WSA)	1979–2012	WDCGG/EC
Mt. Waliguan, CN (WLG)	1990–2013	NOAA/ESRL
Western Pacific Cruise (WPC)	2004–2013	NOAA/ESRL
Ny-Alesund, Svalbard, Norway and Sweden (ZEP)	1994–2013	NOAA/ESRL

ACPD
15, 11889–11923, 2015

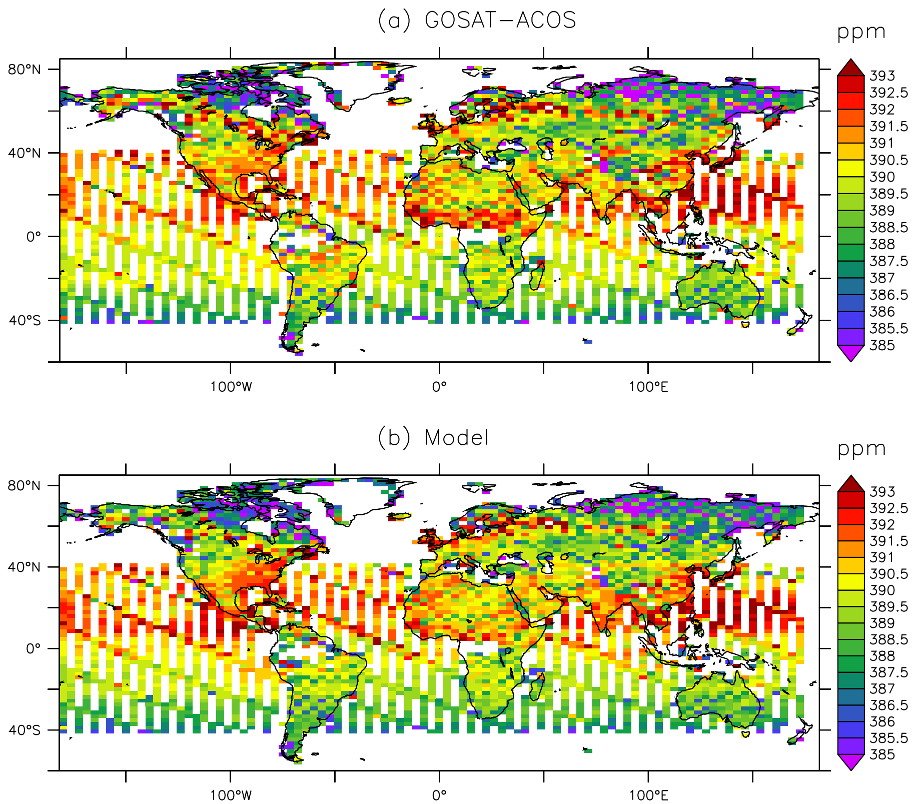

Figure 1. (a) Mean ACOS-GOSAT bias-corrected retrievals in the model grid over 4 years (June 2009–May 2013). **(b)** Corresponding mean CO_2 4-D field associated to the MACC CO_2 inversion (computed using the averaging kernels and the prior profiles of the retrievals).

ACPD
15, 11889–11923, 2015

On the optimality of satellite-based CO_2 atmospheric inversions

F. Chevallier

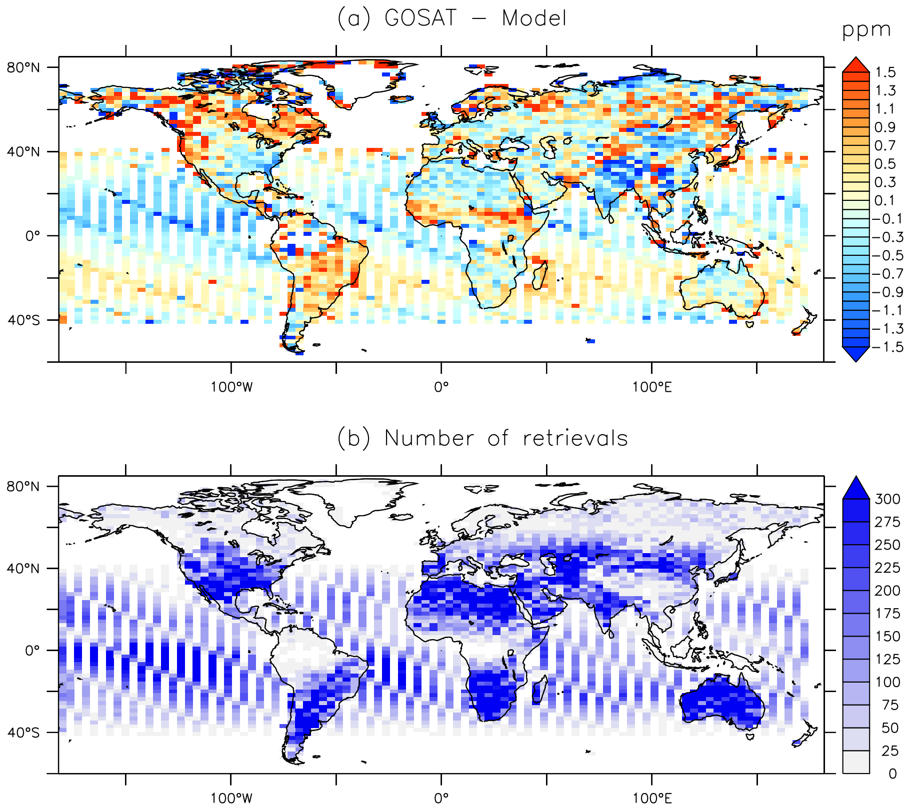

Figure 2. (a) Mean difference between the maps of Fig. 1 (retrievals minus model). **(b)** Corresponding number of retrievals.

ACPD
15, 11889–11923, 2015

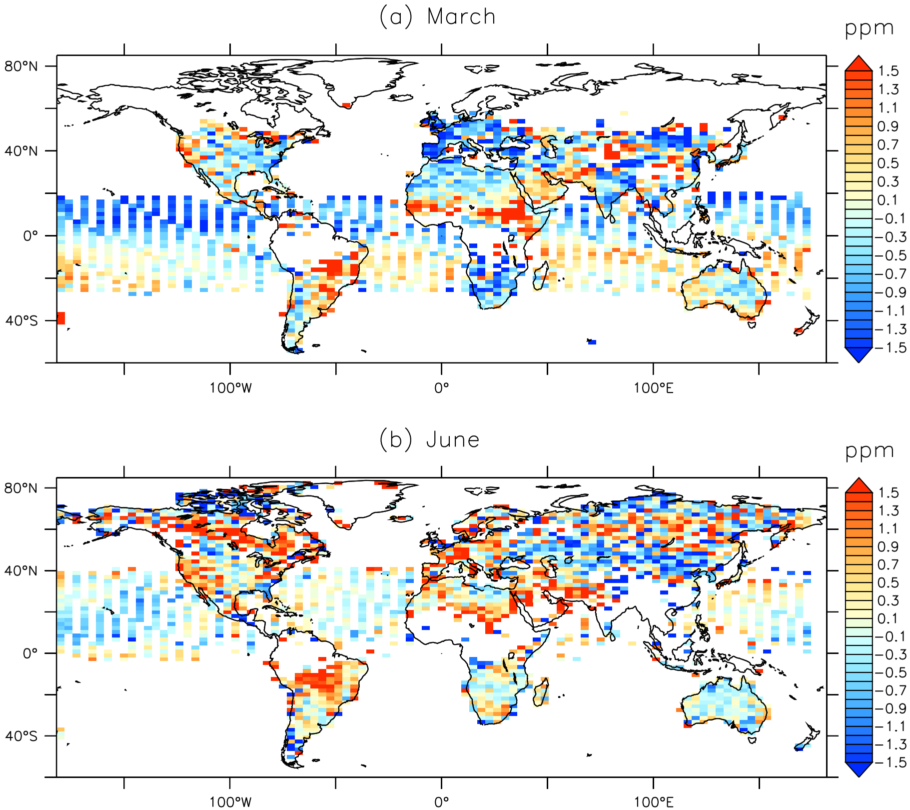

Figure 3. Same as Fig. 2a (retrievals minus model), but focussing on the months of March and June.

ACPD
15, 11889–11923, 2015

On the optimality of satellite-based CO_2 atmospheric inversions

F. Chevallier

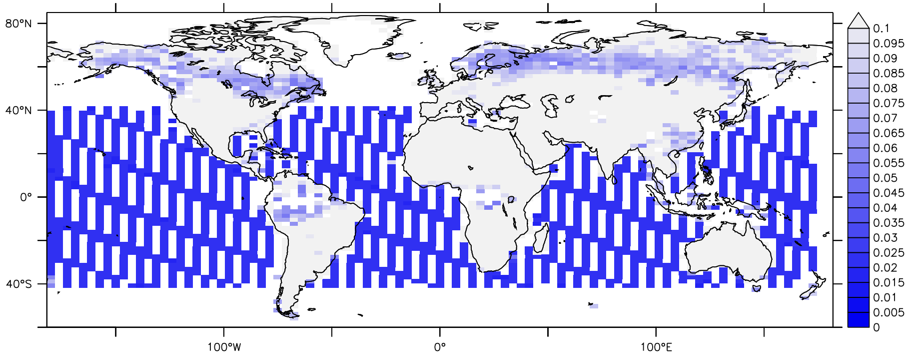

Figure 4. Mean surface albedo retrieved in the strong CO_2 band by ACOS-GOSAT in the model grid over 4 years (June 2009–May 2013). The blue scale focuses on the values less than 0.1.

ACPD
15, 11889–11923, 2015

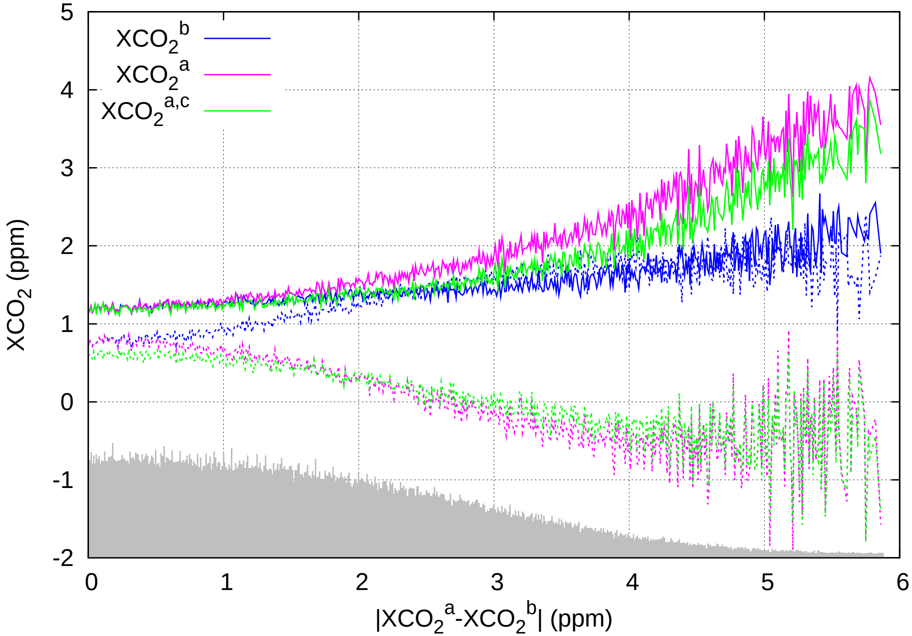

Figure 5. Mean and standard deviation of the retrieval-minus-model misfits between June 2009 and May 2013 for the high-gain mode retrievals over land as a function of the retrieval increment size. The statistics are also shown for the prior-minus-model misfit. The model values are raw pressure-weighted columns and do not account for the averaging kernels in order not to correlate the two axes (in practice, using the averaging kernels actually does not significantly affect the standard deviations shown). The grey shade shows the distribution of the retrieval density (axis not shown).

ACPD
15, 11889–11923, 2015

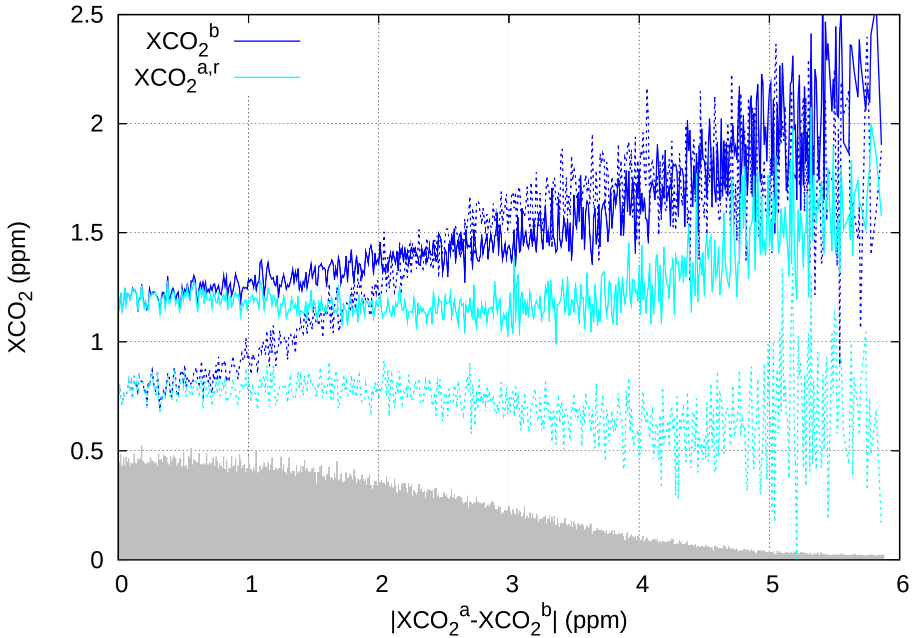

Figure 6. Same as Fig. 5 (high-gain mode over the lands) but we reduce the retrieval increment size by 50 % without any bias correction (we call $XCO_2^{a,r}$ the result). The abscissa shows the unperturbed increment.

ACPD
15, 11889–11923, 2015

On the optimality of satellite-based CO_2 atmospheric inversions

F. Chevallier

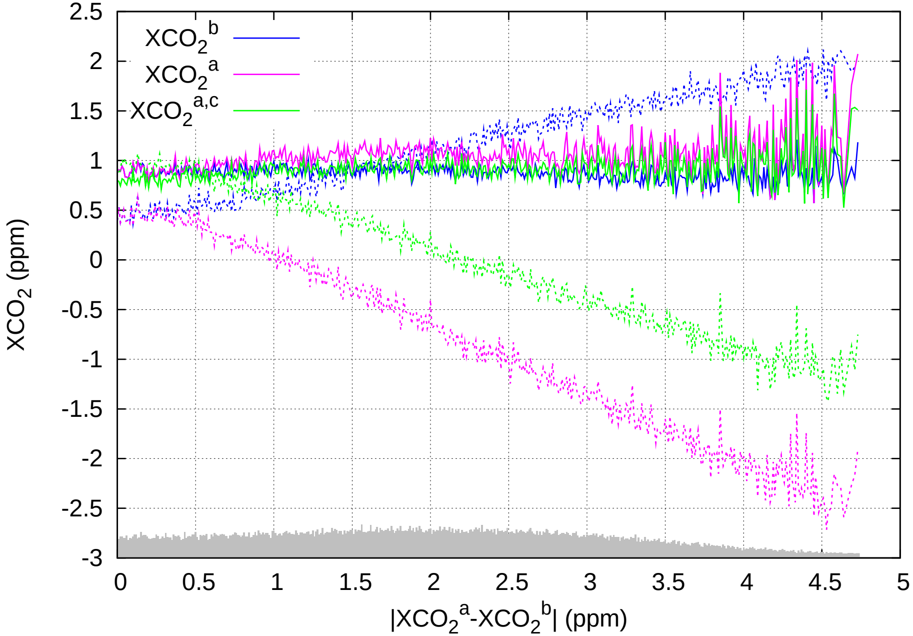

Figure 7. Same as Fig. 5 for the medium-gain mode.

ACPD
15, 11889–11923, 2015

On the optimality of satellite-based CO_2 atmospheric inversions

F. Chevallier

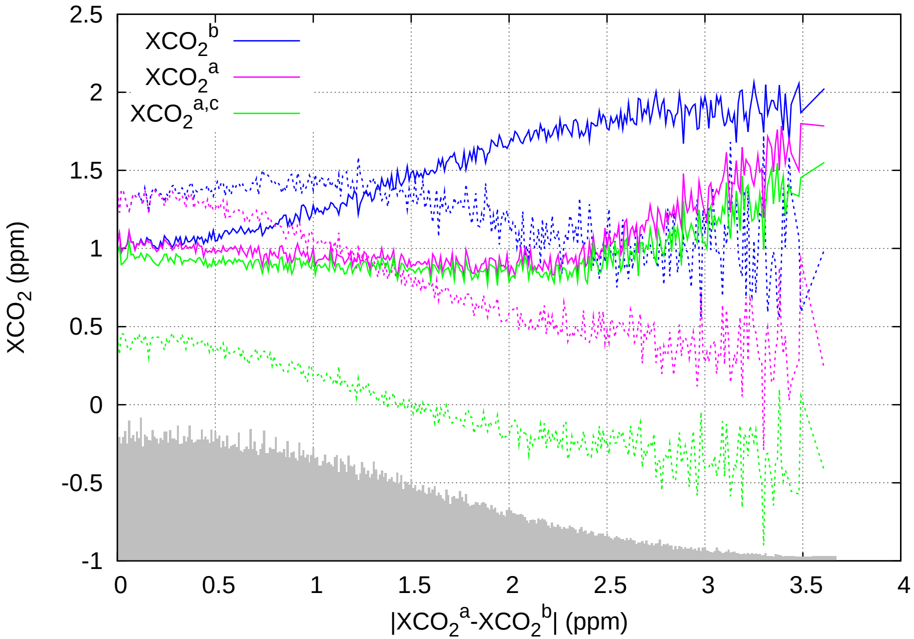

Figure 8. Same as Fig. 5 for the glint mode over the ocean.

ACPD
15, 11889–11923, 2015

On the optimality of satellite-based CO_2 atmospheric inversions

F. Chevallier